Pergamon

Int. J. Solids Structures Vol. 34, No. 29, pp. 3837–3857, 1997

0020–7683/97 $17.00 + .00

PII: S0020–7683(96)00240–5

CRACK-SIZE DEPENDENCE OF OVERALL RESPONSES OF FIBER-REINFORCED COMPOSITES WITH MATRIX CRACKING

A. CHANDRA, Y. HUANG
Department of Mechanical Engineering and Engineering Mechanics, Michigan Technological University, Houghton, MI 49931, U.S.A.

and

K. X. HU
Corporate Software Center, Motorola Inc., Schaumburg, IL 60196, U.S.A.

(*Received* 25 *October* 1995; *in revised form* 15 *November* 1996)

Abstract—Development of a micromechanics model capable of providing overall macroscopic responses for directionally fiber-reinforced composites undergoing matrix cracking (in terms of microgeometric features) is the principal objective of this paper. It is shown that fiber bridging plays an important role, and the effective moduli of a composite may be significantly influenced by the crack size. Bridging effects are negligible for infinitesimally small cracks (or $a \to 0$), and closed-form effective moduli are obtained via standard micromechanics approach for a hybrid composite system with two distinct inclusion phases (fibers and cracks). When crack size exceeds a threshold value a_s (a_s being the crack size for saturated bridging), the bridging effect is significant, and a closed-form solution for effective moduli is again possible using a self-consistent approach accommodating bridging effects within the micromechanics framework. In the transition regime ($0 < a < a_s$), however, the effective moduli become crack-size dependent. A full three-dimensional bridging solution, involving discrete fibers and penny-shaped cracks, is developed to numerically determine the effective moduli in this regime. The procedure also allows numerical determination of the saturated crack size, a_s. The important of crack-size dependence is then discussed. It is observed that the effective longitudinal modulus for a silicon carbide reinforced intermetallic may be significantly underestimated by standard micromechanics model. In the transition range ($0 < a < a_s$), the present model also provides an avenue for estimation of crack sizes based on observations of overall macro-moduli of damaged composite systems. © 1997 Elsevier Science Ltd.

1. INTRODUCTION

Fiber-reinforced ceramic, glass-ceramic, and intermetallic matrix composite materials have received and are receiving a great deal of consideration for high-temperature structural applications. These composites are characterized by matrices that are stiff, compared to conventional polymer-based composites, and that exhibit relatively low overall strain to failure. Brittle matrix composites generally experience damage associated with the matrix and/or interface well before final failure because of the low strain capability of the matrix. Matrix cracking will significantly influence the performance of these composites. When the applied stress exceeds a certain level, known as the microcracked stress level, composites may exhibit environmental interaction and degradation, which, in turn, could accelerate a failure process. One such example is that matrix cracking or interfacial debonding will greatly enhance carbon oxidation. Matrix microcracking is, therefore, a fundamental life-limiting issue for ceramic or intermetallic composites used in high-temperature structural applications.

Both analytical and experimental investigations have been carried out by many investigators in attempts to understand the damage processes in brittle matrix composites under tension parallel to the fiber direction (Aveston *et al.*, 1971; Marshall *et al.*, 1985; McCartney, 1987; Kim and Pagano, 1991; Bao and Suo, 1992). It has been observed that matrix cracking occurs in the direction perpendicular to fibers. After crack nucleation, two modes of damage evolution are possible: multiple cracking and crack extension (Shaw *et al.*, 1993). These two microcracking processes may also be operating simultaneously in a

specific composite. The formation of a multiple cracking zone distributes damage and can significantly influence the stiffness of the composite (Deve and Maloney, 1991; Deve *et al.*, 1992; Hu *et al.*, 1994). As an alternative, one can also focus on overall responses of these composites. The contemporary literature in this area includes several micromechanics models (e.g., Christensen and Lo, 1979; Taya and Chou, 1981; Weng, 1984, 1990; Dvorak, 1986, 1990; Norris, 1985; Benveniste, 1987, 1993; Christensen, 1990; Siboni and Benveniste, 1991; Christensen *et al.*, 1992; Benveniste and Dvorak, 1992; Huang *et al.*, 1994c), whose origin may be traced back to the earlier work by Budiansky (1965) and Hill (1963, 1965). Treatment of hybrid composites with two inclusion phases; reinforcing fibers and matrix cracks, is the direct relevance to the present work. However, only limited work exists in this area (Zhao *et al.*, 1989; Siboni and Benveniste, 1991; Huang *et al.*, 1993; Kachanov, 1993), and the existing micromechanical models are valid for very small crack densities. Accounting for bridging tractions due to fibers, these models may be adapted for cases with very large crack densities. However, they cannot be utilized for an intermediate range of finite crack sizes below saturated bridging levels.

The overall responses of composite systems undergoing matrix cracking are of practical importance for two reasons: (1) they allow the complete history of structural responses to be charted without going through the details of microstructural features (Chandra *et al.*, 1995a, b; Jiang *et al.*, 1996; Huang *et al.*, 1996) and (2) they form the basis of a rational damage mechanics, whereby the effective properties are obtained in terms of damage nucleation and/or growth (Kachanov, 1993). The existing analyses for overall responses of composite systems undergoing matrix cracking suffer the following major drawbacks: First, the bridged-crack models have been established based on two-dimensional plane stress or plane strain conditions but the basic bridging force-displacement relations have been derived by carrying out three-dimensional analyses with fiber size as an explicit working parameter. Therefore, an analytical inconsistency exists between the bridging law and the analysis of a specific bridged-crack system. The consequence of a two-dimensional bridging analysis is that the spatial variation of crack tip behavior is entirely neglected. Second, the bridged-crack systems have been analyzed by embedding a bridged crack in an isotropic material, with effective property derived from the rule of mixture or other micromechanical analyses. The isotropic model may be a good simplification for randomly particulate-reinforced composites, but it is not valid for unidirectionally fiber-reinforced composites. Third, the existing bridging analyses are based on a continuous bridging model. For commonly used fiber-reinforced composites, the fiber volume fraction is less than 40%. For such levels of fiber volume fractions, averaging the fiber-bridging effect in a continuous fashion may not be well justified. Finally, the assumption of small-scale bridging has been adopted. For composites with high fiber strength, a defect-sensitive failure may still exist. As was established by Evans and McMeeking (1986) and Evans (1980), the riding R-curve behavior stems from the transition of large-scale bridging to small-scale bridging. Although not a direct consequence, one would expect similar trends moduli variations as well (see Figs 8a, b). These observations provide the motivation for the current study.

Accordingly, the objective of the present investigation is to develop a general methodology capable of delivering overall elastic responses of fiber-reinforced composites subject to matrix cracking, over the full range of crack densities. The present analysis is based on a three-dimensional, discrete fiber-bridging model capable of accounting for the effects due to material anisotropy. An additional parameter—crack size—is introduced into the micromechanics model to extend validity over the full range of crack densities. It is observed that for infinitesimal crack sizes ($a \to 0$) and for saturated fiber bridging ($a \geqslant a_s$, a_s being critical crack size for saturated bridging), the three-parameter model degenerates to the traditional two parameter model. The full three-parameter model, however, is needed for characterization in the intermediate range $0 < a < a_s$.

Following the introductory section, the crack-size dependence of overall macro-scale moduli is discussed in Section 2. Section 3 presents a set of closed-form solutions for infinitesimally small cracks ($a \to 0$). The overall effective moduli, for saturated bridging ($a \geqslant a_s$) is obtained in Section 4 through a self-consistent approach. The full three-parameter micromechanics model is analyzed numerically in Section 5 for intermediate range involving

finite cracks ($0 < a < a_s$) and unsaturated fiber bridging. The critical crack size a_s for saturated bridging is numerically estimated. Finally, a discussion of the results and their implications are presented in Section 6.

2. CHARACTERIZATION OF A COMPOSITE SYSTEM WITH MATRIX CRACKING

We consider a unidirectionally fiber-reinforced composite subject to matrix cracking. It has been observed by many investigators (e.g., Kim and Pagano, 1991; Shaw *et al.*, 1993) that damage processes occur due to nucleation of matrix cracks in the direction perpendicular to the fibers in a brittle matrix composite (e.g., fiber-reinforced ceramic or glass-ceramic matrix composite materials) under tension parallel to the fiber direction. In accordance with these observations, the microcracks are assumed to be parallel to each other and perpendicular to the fiber direction. Such a material system can be viewed as a hybrid composite with two inclusion phases, one being the unidirectionally aligned fibers and the other (cracks) being a special inclusion of zero modulus. Extensive micromechanical analyses aimed at obtaining the effective mechanical responses of composite materials in terms of those individual composite constituents have been carried out. These include the (generalized) self-consistent method (Budiansky, 1965; Christensen and Lo, 1979; Benveniste, 1992; Huang *et al.* 1994c), differential method (Roscoe, 1952; Norris, 1985; Zimmerman, 1991), and Mori–Tanaka's method (Taya and Chou, 1981; Weng, 1984; Benveniste, 1987). When applied to a composite system of more than one inclusion phase, the micromechanical analysis, however, may not provide a unique solution for composite responses [see Huang *et al.* (1994b) for a detailed discussion]. It is also noted that all the micromechanical models characterize a composite system in terms of a group of constituent distribution parameters.

For the composite system with unidirectional fibers and parallel cracks perpendicular to the fiber direction, a micromechanical analysis gives the effective modulus in the following form [see Huang *et al.* (1993) and further analysis given in Section 3]:

$$\frac{E_3}{E_m} = \frac{E_3}{E_m}(c_f, \rho) \tag{1}$$

when the Young's modulus and Poisson's ratio of the matrix and fibers are given. Here, c_f, the fiber volume fraction, and ρ, termed crack density, are defined as

$$\rho = \frac{N}{V}a^3 \tag{2a}$$

$$c_f = \frac{N_f}{S}a_f^2. \tag{2b}$$

Here, a_f and a are the characteristic average radius of the fibers and cracks (we consider the penny-shaped crack here), N/V is the number of cracks per unit composite volume and N_f/S is the number of fibers per unit area in the transverse plane. The effects of the constituents' geometry (fibers and cracks in the present case) on the effective property are solely embodied by fiber volume fraction and crack density. In other words, one can obtain identical effective moduli for two different microcracked composite systems, one having a large number (high value of N/V) of small cracks (small value of a) and the other with a small number (low value of N/V) of large cracks (high value of a), as long as the combination yields a crack density as defined in eqn (2a). A similar statement holds: The effective property will be unaltered regardless of fiber size if the combination of a_f and N_f/S provides a fiber volume fraction as defined in eqn (2b).

We also note that the solution given in eqn (1) of a microcracked composite system, or more generally of a hybrid composite system, is entirely based on the concept of non-bridged cracks, although it accounts for interactions among fibers and cracks within the framework of a micromechanics model. When cracks are bridged by crossing fibers, as they

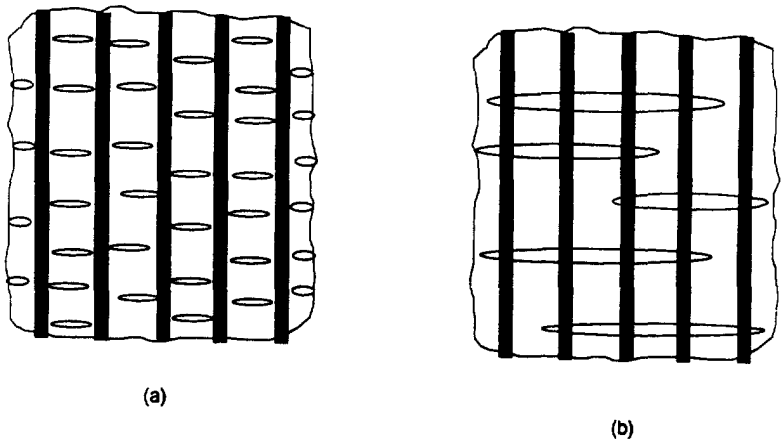

Fig. 1. Schematic diagram for two composite systems with the same crack density: (a) large number of small cracks; (b) small number of large cracks.

are in a general composite system, the micromechanical solution given in eqn (1) is not always valid. As a result, a distinction has to be made between a small number of large cracks and a large number of small cracks. To illustrate this concept we consider two different combinations of crack size and number that provide identical crack densities. Figure 1(a) considers the combination of a large number of small cracks, and Fig. 1(b) that of a small number of large cracks. Apparently, what separates these two configurations from each other is that a significantly higher level of fiber bridging exists for the latter scenario. Due to fiber bridging, crack opening will be reduced and effective responses of the latter configuration will be different from the former, or the one with the small cracks. Therefore, the proper characterization of a microcracked composite system will require consideration of crack size variations that embody the extent of fiber bridging. As discussed above (eqn 2), a simple dimensional analysis led to a possible choice of the scaling constant as a/a_f.

If we assume that the fibers inside the penny-shaped crack are not broken [not in a steady state for the crack tip behavior as defined by Budiansky *et al.* (1988)] and can all be used as bridging agents, the bridging effect is expected to reach a limit when crack size becomes significantly large, i.e., the saturated crack size, a_s. When the crack size is larger than a_s, the effective modulus is expected to become insensitive to crack-size, again. This observation will be confirmed later in Section 5 through numerical analysis.

These conceptual observations lead us to conclude that the effective responses of a fiber-reinforced composite with matrix cracking can be determined in terms of fiber volume fraction and crack density if the cracks are infinitesimal ($a \to 0$) or $a \geqslant a_s$. In other words, a two-parameter characterization is valid when either the crack size is infinitesimally small such that the bridging effect can be neglected or the crack size is so large that the extent of bridging is saturated. The overall responses are, however, dependent on crack size when crack size falls in between these values. Therefore, the complete solution for the effective modulus shall be expressed in the form

$$\frac{E_3}{E_m} = \frac{E_3}{E_m}(c_f, \rho) \quad a \to 0 \tag{3a}$$

$$\frac{E_3}{E_m} = \frac{E_3}{E_m}\left(c_f, \rho, \frac{a}{a_f}\right) \quad 0 < a < a_s \tag{3b}$$

$$\frac{E_3}{E_m} = \frac{E_3}{E_m}(c_f, \rho) \quad a > a_s. \tag{3c}$$

It should be noted that, even though the moduli for the cases $a \to 0$ and $a > a_s$ can be characterized by c_f and ρ, the functionality form of the solution is different for each, with

a non-bridging effect for $a \to 0$ and a saturated bridging effect for $a > a_s$. The main theme in what follows is the determination of the specific form of the modulus solution for a corresponding crack-size range. The saturated crack size, a_s, is obtained during the solution process. It is worthwhile to mention in passing that within the transition range, or $0 < a < a_s$, a physical bridging model will enter the equation and the solution may become quite complex. As will become clear in Section 5, the solution can indeed be expressed in the form of eqn (3b) when bridging is effective.

3. SOLUTIONS FOR INFINITESIMAL MATRIX CRACKS ($a/a_f \ll 1$)

A fiber-reinforced composite containing small-sized matrix cracks, $a/a_f \ll 1$, is investigated first. As discussed before, the effect of fiber bridging for the case of small crack size is insignificant. Therefore, the solution for a fiber-reinforced composite containing small-sized matrix cracks can be obtained by treating the composite as a material with two phases of inclusions, one being the reinforcing fibers and the other being cracks. A micromechanics approach, using Mori–Tanaka's average technique, will be adapted in the present study. A micromechanics analysis, when employed for solution of effective properties, involves two ingredients; a proper stress–strain definition and a geometric model accounting for phase interactions. The stress–strain relationship for overall composite responses can be addressed by a direct approach (Benveniste, 1987) or by an energy equivalence approach (Budiansky, 1965; Huang *et al.* 1993). When used for hybrid composites with coexisting reinforcements and cracks, the energy approach has been proven to be advantageous since crack energy can be evaluated through the concept of an energy release rate (Budiansky and O'Connell, 1976; Huang *et al.* 1993). In the following, an energy balance framework will be utilized and adapted to the Mori–Tanaka average technique in order to obtain the solution for effective composite properties.

Consider a large block of composite material comprised of reinforcing fibers in the x_3 direction and a system of small-sized parallel matrix cracks in the direction perpendicular to the fibers. The fibers are assumed to be cylindrical and are randomly distributed in the x_1–x_2 plane. The cracks are assumed to be penny-shaped and are randomly distributed in planes perpendicular to the fiber direction. The elastic modulus and Poisson's ratio of the matrix are E_m and ν_m, and those of the fibers are E_f and ν_f. Due to the aligned distribution of fibers and crack, the composite shows an orthotropic behavior and can be characterized by the following general stress–strain relation:

$$\sigma_{ij} = C_{ijkl}\varepsilon_{kl} \quad \text{or } \varepsilon_{ij} = C^{-1}_{ijkl}\sigma_{kl} \tag{4}$$

where C_{ijkl} is the elastic moduli tensor of the composite material. In order to determine C_{ijkl} or its inverse (tensor of elastic constants), apply a uniform stress, $\sigma_{ij} = \sigma^0_{ij}$, to the surface of the block of composite material. The strain energy of the composite material is, from the homogenization, given as

$$U = \tfrac{1}{2} C^{-1}_{ijkl}\sigma^0_{ij}\sigma^0_{kl}V \tag{5}$$

where V is the total volume of the composite material. On the other hand, one can view the strain energy from each individual phase. For a composite system with inclusions and cracks, the strain energy can be given as (Huang *et al.*, 1993)

$$U = \frac{1}{2}\left\{\frac{1+\nu_m}{E_m}\sigma^0_{ii}\sigma^0_{jj} - \frac{\nu_m}{E_m}\sigma^0_{ii}\sigma^0_{jj} + c_f\left[\left(1 - \frac{1+\nu_m}{1+\nu_f}\frac{E_f}{E_m}\right)\sigma^0_{ij}\varepsilon^f_{ij} + \frac{\nu_m - \nu_f}{(1-2\nu_f)(1+\nu_f)}\frac{E_f}{E_m}\sigma^0_{ii}\varepsilon^f_{jj}\right]\right\}V + \sum_{i=1}^{N}\iint_{S_i} G(S)\,\mathrm{d}S \tag{6}$$

where $\varepsilon^f_{ij} = 1/V_f\int_{V_f}\varepsilon j\,\mathrm{d}V$ is the average fiber strain, $G(r)$ is the energy release rate of a

penny-shaped crack of radius r under the specified loading condition, S_i is the area of a particular crack in the composite block, and N is the number of cracks in that block. The last term in eqn (6) represents the total crack energy in the block. By energy equivalence, we have, from eqns (5) and (6),

$$C^{-1}_{ijkl}\sigma^0_{ij}\sigma^0_{kl} = \frac{1+\nu_m}{E_m}\sigma^0_{ij}\sigma^0_{ij} = \frac{\nu_m}{E_m}\sigma^0_{ii}\sigma^0_{jj} + c_f\left[\left(1+\frac{1+\nu_m}{1+\nu_f}\right)\sigma^0_{ij} - \varepsilon^f_{ij} + \frac{\nu_m-\nu_f}{(1-2\nu_f)(1+\nu_f)}\frac{E_f}{E_m}\sigma^0_{ii}\varepsilon^f_{jj}\right] + \frac{N}{V}\int_0^a G(r)2\pi r\,\mathrm{d}r \quad (7)$$

where a is the average crack radius; obviously, for the small crack size considered here, $a/a_f \ll 1$.

Equation (7) is an exact representation of the energy equivalence between two views of the cracked composite: one regards the composite as an effective, homogeneous medium, and the other considers the details of the individual phases—the matrix, fibers and cracks. In order to determine the effective property of the microcracked composites, or C_{ijkl}, a scheme for obtaining average fiber strain, as well as the crack energy release rate, has to be developed to approximately account for interactions among the matrix, fibers and cracks. It is this scheme (the second ingredient of a micromechanics model) for evaluating the average fiber strain and crack energy release rate that introduces a variety of approximations associated with a micromechanics model. Two schemes, the Mori–Tanaka method (e.g., Taya and Chou, 1981; Weng, 1984, 1990; Benveniste, 1987) and the inclusion-matrix-composite model, also referred to as the generalized self-consistent method (e.g., Christensen and Lo, 1979; Benveniste, 1986; Siboni and Benveniste, 1991; Huang *et al.*, 1994a, c), have gained a wide range of acceptance. These two schemes are competing in some applications and complementary in others [see Christensen (1990), Wang and Weng (1992), and Huang *et al.* (1994b) for detailed discussions on their comparisons]. In what follows, we use the Mori–Tanaka method to evaluate the average fiber strain and crack energy release rate. It is noted here that the Mori–Tanaka method is relatively simple in terms of providing closed-form solutions, it is unambiguous in terms of accommodating multiphase inclusions (as is certainly the case for the microcracked composite under consideration), and it has the typical features of a micromechanics model. These features will be modified as they will be shown to be insufficient as the extent of fiber bridging increases (see Section 5).

In order to implement the Mori-Tanaka method, we apply a remote stress, $\sigma_{33} = \sigma_0$ ($\sigma^0_{ij} = 0$, otherwise), as shown in Fig. 2(a). (The aligned ellipsoidal inclusions are used so

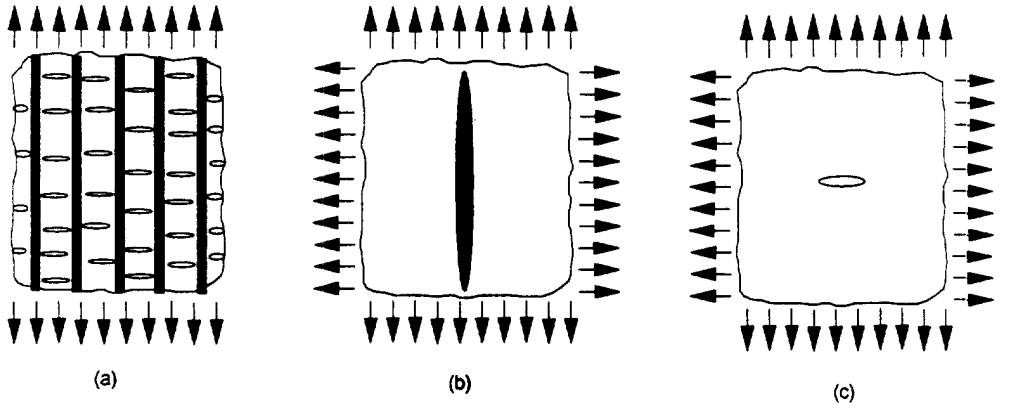

Fig. 2. An interpretation of Mori–Tanaka's method for small-sized cracks: (a) the composite system with small-sized matrix cracking subject to uniaxial tension; (b) the configuration providing a relationship between average matrix stresses and average fiber stresses. Note that a triaxial average matrix stress state exists even when the remote tension in the composite system is uniaxial; (c) the configuration providing a relationship between average matrix stress and the average crack energy release rate.

that a solution for the long, cylindrical fibers can be derived by taking the limit of the aligned ellipsoidal axis to infinity.) The average stresses of the matrix material in the composite system will be developed due to the remote stress $\sigma_{33} = \sigma_0$. The state of the average matrix stress is not necessarily coaxial with the remote stress; it is, however, axisymmetric and can be expressed as $(\sigma_{11}^{mx}, \sigma_{22}^{mx}, \sigma_{33}^{mx})$. The average fiber stress can be characterized, by reasoning, as $(\sigma_{11}^{fb}, \sigma_{22}^{fb}, \sigma_{33}^{fb})$. One can show that the average stress in cracks, in a limit sense is zero (Benveniste, 1987; Zhao *et al.*, 1989). The stress equilibrium then requires

$$(1-c_f)\begin{pmatrix}\sigma_{11}^{mx}\\ \sigma_{33}^{mx}\end{pmatrix}+c_f\begin{pmatrix}\sigma_{11}^{fb}\\ \sigma_{33}^{fb}\end{pmatrix}=\begin{pmatrix}0\\ \sigma_0\end{pmatrix}. \tag{8}$$

The key assumption of Mori–Tanaka's method used to contain the average fiber stress and crack energy release rate is described in Fig. 2(b, c). This shows that the average fiber stress and crack energy release rate can be obtained by embedding a single typical fiber and a single penny-shaped crack in an infinitely extended matrix material subject to the average matrix stress state $(\sigma_{11}^{mx}, \sigma_{22}^{mx}, \sigma_{33}^{mx})$. The average fiber stresses $(\sigma_{11}^{fb}, \sigma_{22}^{fb}, \sigma_{33}^{fb})$ can be related to $(\sigma_{11}^{mx}, \sigma_{22}^{mx}, \sigma_{33}^{mx})$ through the solution of the single-fiber system shown in Fig. 2(b). After inverting the readily derivable single-fiber solution given by Mura (1982), we have

$$\begin{pmatrix}\sigma_{11}^{mx}\\ \sigma_{33}^{mx}\end{pmatrix}=\begin{bmatrix}m_{11}, m_{13}\\ m_{31}, m_{33}\end{bmatrix}\begin{pmatrix}\sigma_{11}^{fb}\\ \sigma_{33}^{fb}\end{pmatrix} \tag{9}$$

where

$$m_{11} = \tfrac{1}{2}\{1-v_m+\beta[1-(1+2v_m)v_i]\} \tag{10a}$$

$$m_{13} = \tfrac{1}{2}\beta(v_m-v_i) \tag{10b}$$

$$m_{31} = \frac{v_m}{1-v_m}+\beta[v_m-(2+v_m)v_i] \tag{10c}$$

$$m_{33} = \beta(1-v_m v_i) \tag{10d}$$

$$\beta = \frac{E_m}{E_1(1-v_m^2)}. \tag{10e}$$

Substituting eqn (9) into eqn (8), we have

$$\begin{pmatrix}c_f+(1-c_f)m_{11} & (1-c_f)m_{13}\\ (1-c_f)m_{31} & c_f+(1-c_f)m_{33}\end{pmatrix}\begin{pmatrix}\sigma_{aa}^{fb}\\ \sigma_{33}^{fb}\end{pmatrix}=\begin{pmatrix}0\\ \sigma_0\end{pmatrix}. \tag{11}$$

The solution of eqn (11) leads to

$$\frac{\sigma_{11}^{fb}}{\sigma_0} = -\frac{c_m}{2\gamma}(v_m-v_i)\beta \tag{12}$$

$$\frac{\sigma_{33}^{fb}}{\sigma_0} = \frac{1}{\gamma}\left\{c_f+\frac{c_m}{2}\left[\frac{1}{1-v_m}+\beta(1-v_i-2v_m v_i)\right]\right. \tag{13}$$

$$\frac{\sigma_{11}^{mx}}{\sigma_0} = \frac{\sigma_{22}^{mx}}{\sigma_0} = \frac{\gamma}{2\gamma}(v_m-v_i)\beta \tag{14}$$

$$\frac{\sigma_{33}^{mx}}{\sigma_0} = \frac{1}{c_m}\left(1-\frac{c_f^2}{\gamma}\right) - \frac{c_f}{\gamma}\left[\frac{1}{1-\nu_m} + \beta(1-\nu_i - 2\nu_m\nu_i)\right] \tag{15}$$

where

$$\gamma = \frac{c_m^2}{2}\beta(\nu_m-\nu_i)\left[\frac{\nu_m}{1-\nu_m} + \beta(\nu_m - 2\nu_i - \nu_m\nu_i)\right] + [c_f + c_m\beta(1-\nu_m\nu_i)]x\left\{c_f + \frac{c_m}{2}\left[\frac{1}{1-\nu_m} + \beta(1-\nu_i-2\nu_m\nu_i)\right]\right\} \tag{16}$$

and the crack energy release rate is found to be [see Fig. 2(c)]

$$G(r) = \frac{1-\nu_m^2}{E_m}\frac{4}{\pi}(\sigma_{33}^{mx})^2 r. \tag{17}$$

With the solution of the average fiber stresses (or strains) and the crack energy release rate in hand, the governing equation (eqn 7) for the determination of effective moduli can be implemented, giving

$$\frac{1}{E_3} = \frac{1}{E_m} + c_f\left\{\frac{1}{2}\left(\frac{1}{G_f}-\frac{1}{G}\right)\frac{\sigma_{33}^{fb}}{\sigma^0} + \left(\frac{\nu_m}{E_m}-\frac{\nu_f}{E_f}\right)\frac{\sigma_{11}^{fb}+\sigma_{22}^{fb}+\sigma_{33}^{fb}}{\sigma^0}\right\} + \frac{16(1-\nu_m^2)}{3E_m}\rho\left(\frac{\sigma_{33}^{fb}}{\sigma_0}\right)^2 \tag{18}$$

where ρ is crack density (Budiansky and O'Connell, 1976; Kachanov, 1993) as defined in eqn (2a).

While eqn (18), along with eqns (12)–(15), provides a complete solution for the longitudinal modulus E_3, further simplification is possible. The final result is found to be

$$\frac{E_3}{E_m} = \left\{\left[c_m + c_f\left(\frac{E_f}{E_m} + \frac{4c_fc_m(\nu_f-\nu_m)^2}{E_m(c_f/\bar{K}_m + c_m/\bar{K}_f + 1/G_m)}\right)\right]^{-1} + \frac{16}{3}\rho(1-\nu_m^2)x\left[\frac{1}{c_m}\left(1-\frac{c_f^2}{\gamma}\right) - \frac{c_f}{2\gamma}\left(\frac{1}{1-\nu_m} + \beta(1+\nu_i-2\nu_m\nu_i)\right)\right]^2\right\}^{-1} \tag{19}$$

where G_m and $\bar{K}_m$ are the shear and in-plane bulk moduli of the matrix material and $\bar{K}_f$ are the in-plane bulk moduli of the fibers.

Similarly, the in-plane shear, G_{13}, can be determined by applying a remote stress, $\tau_{13} = \tau_0$ (otherwise = 0). The solution for the relationship between τ_{13}^{fb} and τ_{13}^{mx} (the average shear stress of the matrix and fibers due to the remote stress τ_0) can be found by embedding an isolated fiber into an infinitely extended matrix material subject to remote stress τ_{13}^{mx},

$$\sigma_{13}^{mx} = \tfrac{1}{2}(1+\lambda)\sigma_{13}^{fb} \tag{20}$$

where $\lambda = G_f/G_m$. It should be noted here that, unlike the case for uniaxial tension, the applied remote shear stress, τ_{12} $(=\tau_0)$, does not produce any other average stress components. The stress balance requires

$$c_m\sigma_{13}^{mx} + c_f\sigma_{13}^{fb} = \tau^0. \tag{21}$$

Equations (20) and (21) give

$$\frac{\sigma_{13}^{fb}}{\tau_0} = \frac{1}{c_f + \frac{c_m}{2}(1+\lambda)} \tag{22}$$

$$\frac{\sigma_{13}^{mx}}{\tau_0} = \frac{1}{2}\frac{1+\lambda}{c_f + \frac{c_m}{2}(1+\lambda)}. \tag{23}$$

With care taken in the evaluation of the energy release rate for the loading conditions in shear, the governing equation (eqn 7) becomes

$$\frac{1}{G_{13}} = \frac{1}{G_m} + c_f\left(\frac{1}{G_f} - \frac{1}{G_m}\right)\frac{\tau_{13}^{fbn}}{\tau_0} + \frac{16}{3}\frac{1-\nu_m}{2-\nu_m}\frac{\rho}{G_m}\left(\frac{\tau_{13}^{mx}}{\tau_0}\right)^2. \tag{24}$$

Substituting eqns (22) and (23) into eqn (24), the final result is

$$\frac{G_{13}}{G_m} = \left\{1 + \frac{c_f(\lambda-1)}{c_f + \frac{c_m}{2}(\lambda+1)} + \frac{4}{3}\frac{1-\nu_m}{2-\nu_m}\rho\left[\frac{1+\lambda}{c_f + \frac{c_m}{2}(1+\lambda)}\right]^2\right\}^{-1}. \tag{25}$$

4. VERY LARGE MATRIX CRACKS WITH SATURATED FIBER BRIDGING

When large-sized cracks develop, the fibers will bridge across the cracks and, as described in Section 2, the geometric intersections of fibers and cracks will create a feature that is distinct from that of small-sized matrix cracks. First, the bridging fibers falling inside a crack will exert a distribution of closing tractions over the area of a crack where a fiber exists. Second, the fibers inside a crack are not entirely immersed in the surrounding matrix material, as shown in Section 3 [see Fig. 2(b)]. Those fibers falling inside a crack will remain surrounded by the matrix material, with the exception that a free exposition of the fiber surface occurs along the crack opening. One important assumption of the present study is that the effect of the fiber exposition is neglected. Therefore, we can still consider the fibers as being entirely surrounded by matrix material. When crack opening displacements are small in comparison to fiber length, as they are for most fiber-reinforced composite systems, the effect of fiber exposition is marginal. In order to account for the effect of fiber bridging on crack opening displacements, and virtually on the effective moduli, the energy equivalence equation should be modified. The modified Mori–Tanaka scheme is shown in Fig. 3. The difference between Fig. 2 and Fig. 3 is that a typical crack surface is imposed with a distribution of closing tractions (or bridging forces) in Fig. 3. Although the average matrix stresses can still be evaluated following the procedures detailed in Section 3, now the crack energy release rate will also depend on the average matrix stress and the bridging tractions.

Referring to Fig. 3(a), if one cuts the fibers along a crack plane, a pair of opposite tractions appears on the cut fiber sections. It is noted that these tractions are the bridging forces shown in Fig. 3(c). Keep in mind that the bridging traction can be approximated as the average fiber axial stress. We further obtain bridging tractions due to discrete fibers uniformly distributed over the penny-shaped crack. The uniform bridging tractions obtained are

$$\frac{\sigma_b}{\sigma_0} = c_f\sigma_{33}^{fb} = \frac{1}{\gamma}\left\{c^2 + \frac{c_f c_m}{2}\left[\frac{1}{1-\nu_m} + \beta(1-\nu_i-\nu_f\nu_i)\right]\right\}. \tag{26}$$

The energy release rate is then found to be

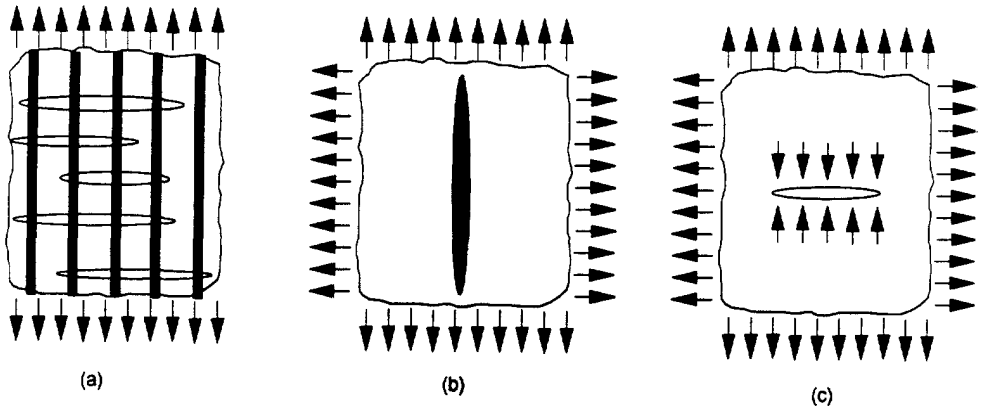

Fig. 3. A modification of Mori–Tanaka's method for large-sized cracks: (a) the composite system with large-sized matrix cracking subject to uniaxial tension; (b) the configuration providing a relationship between average matrix stresses and average fiber stresses. Note that the effect of the intersection of fibers with cracks is neglected; (c) the configuration providing a relationship between average matrix stresses and the average crack energy release rate. Note that the bridging tractions supplied by discreet fibers [Fig. 3(a)] are allotted to a typical crack as a uniform distribution of magnitude $c\sigma_{33}^{fb}$.

$$G(r) = \frac{1-\nu_m^2}{E_m}\frac{4}{\pi}(\sigma_{33}^{mx} - c_f\sigma_{33}^{hf})^2 r. \tag{27}$$

The effective longitudinal modulus can be obtained in a similar manner:

$$\frac{E_3}{E_m} = \left\{\left[c_m + c_f\left(\frac{E_f}{E_m} + \frac{4c_f c_m(\nu_f-\nu_m)^2}{E_m(c_f/\bar{K}_m + c_m/K_m + 1/G_m)}\right)\right]^{-1} + \frac{16}{3}(1-\nu_f^2)x\left[\frac{1}{c_m}\left(1-\frac{c_f^2}{\gamma}\right) - \frac{c_f^2}{\gamma} - \frac{1-c_m^2}{2\gamma}\left(\frac{1}{1-\nu_m} + \beta(1-\nu_i-2\nu_m\nu_i)\right)\right]^2\right\}^{-1}. \tag{28}$$

Similarly, the in-plane shear modulus, G_{13}, can be determined by substituting $(\tau_{13}^{mx} - c_f\tau_{13}^{fb})$ for τ_{13}^{mx} in eqn (24), giving

$$\frac{G_{13}}{G} = \left\{1 + \frac{c_f(\lambda-1)}{c_f + \frac{c_m}{2}(\lambda+1)} + \frac{4}{3}\frac{1-\nu_m}{2-\nu_m}\rho\left[\frac{\frac{1}{2}(1+\lambda)-c_f}{c_f + \frac{c_m}{2}(1+\lambda)}\right]^2\right\}^{-1}. \tag{29}$$

The solutions given in eqns (28) and (29) are a modification of the standard micromechanics solutions given in eqns (19) and (25). This modification provides one possible avenue, based entirely on a micromechanics model, to account for the effect of fiber bridging. The main theme in deriving the solution is to distribute, over cracks, the bridging tractions that are self-consistent with the average fiber stresses obtained by a micromechanics analysis.

As an example, we consider a composite of SiC/BMAS (barium magnesium aluminosilicate) with $E_m = 100$ GPa, $\nu_m = 0.24$, $E_f = 200$ GPa, and $\nu_f = 0.2$. This is one of the SiC-reinforced ceramics in which relatively large cracks can develop to the stage of bridging saturation (Kim and Pagano, 1991). In such cases, the modified solution presented in this section is applicable. The effective longitudinal and shear moduli are shown in Fig. 4(a, b) for crack density $\rho = 0.3$. It is observed that the modified solution (considering the effect of fiber bridging) can differ profoundly from that of the standard micromechanics analysis. For instance, the normalized longitudinal and in-plane shear moduli obtained by the modified solution are 1.34 and 1.15 at a fiber volume fraction of $c_f = 40\%$ as compared to 0.67 and 0.78 by the standard micromechanics analysis.

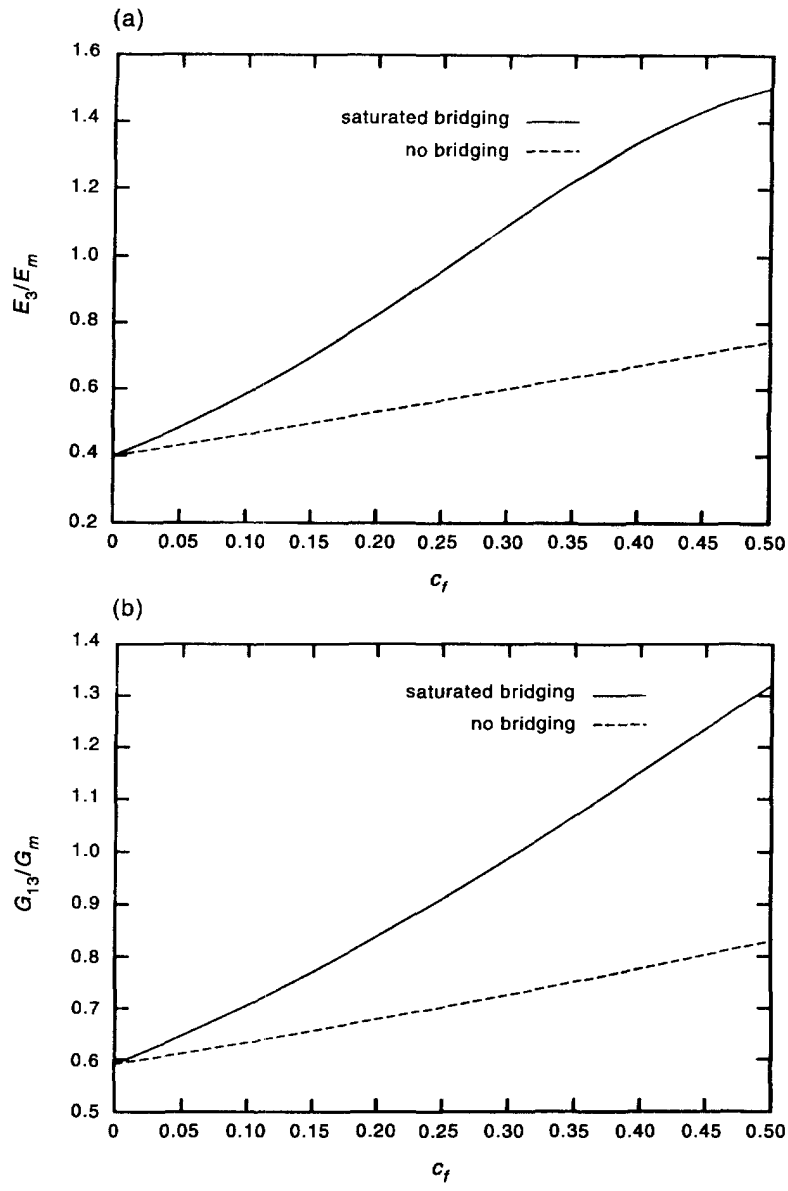

Fig. 4. Comparisons between the solutions for a small-sized crack (without bridging) and those for a large-sized crack (with bridging) for SiC/BMAS with $E_m = 100$ GPa, $\nu_m = 0.24$, $E_f = 200$ GPa, and $\nu_f = 0.2$: (a) longitudinal Young's modulus; (b) in-plane shear modulus.

It should be noted that the modified micromechanics solution provides a self-consistent approach to accommodating the bridging effect within a micromechanics framework. When the crack size is larger than the saturated crack size, the solution, as observed earlier, is still expressible through a two-parameter characterization. The model, however, does not consist of any physical input for the development of bridging. This issue will be addressed in the next section, where a full bridging solution with a bridging law governing relevant mechanisms will be obtained. Also, our analysis shows that the modified micromechanics solution applies to most SiC-reinforced ceramics within a commonly used fiber volume fraction range of up to 40%. There are cases (with combinations of constituent properties and high volume fraction) that may produce negative values of $(\sigma_{33}^{mx} - c_f\sigma_{33}^{fb})$ or $(\sigma_{13}^{mx} - c_f\sigma_{13}^{fb})$. This implies that cracks are not opened based on the micromechanics solution. A simple approach to account for this is to discard the crack influence term in eqns (28) and (29) when cracks are not open. Other approaches include the consideration of fiber stress variations in the axial direction.

5. EFFECT OF FIBER BRIDGING: CRACK-SIZE DEPENDENCE

As discussed in Section 2, in addition to crack density and fiber volume fraction, a third scaling constant, a/a_f, will have to be introduced for the quantitative assessment of effective moduli. To put this reasoning into a rigorous analysis, the key is to determine the bridging tractions. In the following, we will first introduce a three-dimensional, discrete fiber model to analyze a fiber-bridged crack system. A simplified solution for bridging tractions will be presented next. The implications of the results for effective moduli are discussed, and the crack energy release rate is evaluated.

5.1. *A discrete fiber model*

The focus here is to provide the solution of bridging transactions for a penny-shaped crack subject to average matrix stresses [shown in Fig. 3(c)]. The details of fiber distribution inside the penny-shaped crack to be considered since the bridging tractions exist over only those areas where a fiber exists. Representative fiber patches inside a penny-shaped crack are shown in Fig. 5, and bridging tractions are imposed over these fiber patches. The bridging tractions over each patch area are as yet unknown and may vary with the position inside each fiber patch. We assume that a linear bridging law exists such that the bridging traction, σ, can be related to the crack opening displacement, u, through the following relationship:

$$u = K\sigma \tag{30}$$

where K is the proportionality constant. The crack opening displacement under the average matrix stress, σ_{33}^{mx}, and bridging tractions can be written as (Fabrikant, 1989; Gao and Rice, 1987)

$$w(\rho,\phi) = 4H\sigma_{33}^{mx}(a^2-\rho^2)^{1/2} - \frac{2}{\pi}H\sum_{i=1}^{N}\iint_{S_i}\frac{\sigma_i(\rho_0,\phi_0)}{R}\tan^{-1}\left(\frac{\eta}{R}\right)\rho_0\,\mathrm{d}\rho_0\,\mathrm{d}\phi_0 \tag{31}$$

where $\sigma_i(\rho_0,\phi_0)$ represents the as yet unknown bridging traction distribution over the ith fiber patch, S_i is the area of the ith patch, the integration is carried out over all N patches

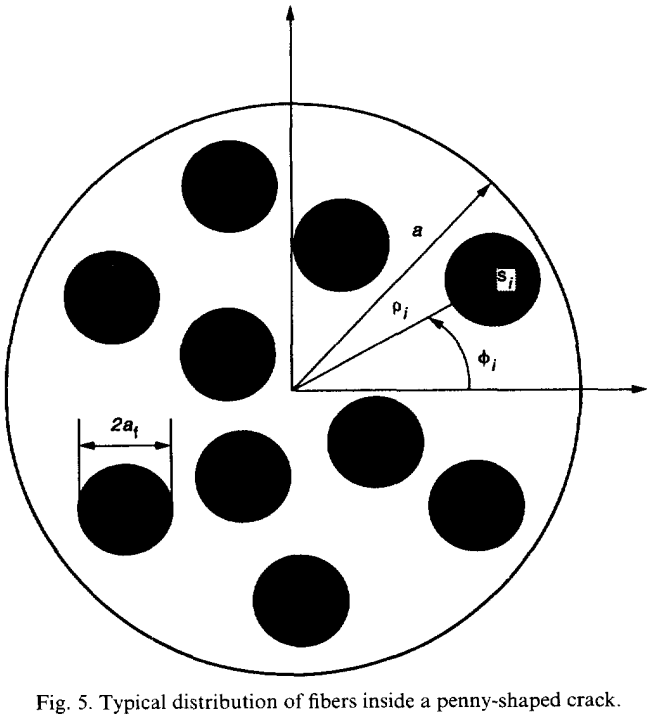

Fig. 5. Typical distribution of fibers inside a penny-shaped crack.

inside the penny-shaped crack in order to account for the total crack opening contribution from all the bridging fiber patches, and

$$R = [\rho^2 + \rho_0^2 - 2\rho\rho_0 \cos(\phi - \phi_0)]^{1/2} \tag{32}$$

$$\eta = \frac{[(a^2 - \rho^2)(a^2 - \rho_0^2)]^{1/2}}{a} \tag{33}$$

$$H = \frac{1 - \nu^2}{\pi E}. \tag{34}$$

Imposing the bridging law over all the fiber patches, we have the following normalized governing equation:

$$4\left[\left(\frac{a}{a_f}\right)^2 - \left(\frac{\rho}{a_f}\right)^2\right]^{1/2} - \frac{2}{\pi}\sum_{i=1}^{N}\iint_{S_i}\frac{\sigma_i(\rho_0, \phi_0)}{\sigma_{33}^{mx}}\tan^{-1}\frac{\eta}{R}\frac{\rho_0\,\mathrm{d}\rho_0\,\mathrm{d}\phi_0}{Ra_f} = \xi\sigma_j(\rho, \phi)$$

$$(\rho, \phi) \in S_j = 1, \ldots, N \tag{35}$$

where ξ is a dimensionless configuration constant,

$$\xi = \frac{K}{Ha_f}. \tag{36}$$

The bridging strength increases as the value of ξ decreases; ξ varies over a wide range, depending on the particular bridging configuration. To solve for the unknown bridging tractions, $\sigma_i(\rho_0, \phi_0)$, we assume that

$$\sigma_i(\rho_0, \phi_0) = \sum_{n=0}^{M}\sum_{m=0}^{M} r^m(a_{mn}\cos n\theta + b_{mn}\sin n\theta) \tag{37}$$

where (r, θ) are the local polar coordinates associated with the ith fiber, a_{mn} and b_{mn} are the unknown coefficients, and M is the number of terms, which is truncated for the purpose of convergence. Equation (35) can then be solved by satisfying the integral equation at a sufficient number of collocation points. It is noted, however, that the integration becomes singular due to $R \to 0$ when $S_i = S_j$. The integration singularity can be removed by transforming the coordinates (ρ_0, ϕ_0) to (ρ_0', ϕ_0') as follows:

$$\rho_0 \cos\phi_0 = \rho_0' \cos\phi_0' + \rho\cos\phi \tag{38a}$$

$$\rho_0 \sin\phi_0 = \rho_0' \sin\phi_0' + \rho\sin\phi. \tag{38b}$$

In the numerical implementation, the collocation points should be evenly distributed over each fiber in order to secure a spatially smooth, convergent solution. Our numerical calculations show that very accurate bridging transactions with relative errors of less than 5% can be obtained with truncation terms of $M = 6$ for fiber densities up to 40% in all three subsequently considered examples.

The normalized stress intensity factor (SIF) can be obtained in terms of bridging tractions following an approach by Cherepanov (1979):

$$\frac{K(\phi)}{K_0} = 1 - \frac{1}{2\pi a}\sum_{i=1}^{N}\iint_{S_i}\frac{\sigma_i(\rho_0, \phi_0)}{\sigma_{33}^{mx}}\frac{(a^2 - \rho_0^2)^{1/2}\rho_0\,\mathrm{d}\rho_0\,\mathrm{d}\phi_0}{a^2 - \rho_0^2 - 2a\rho_0\cos(\phi - \phi_0)} \tag{39}$$

where $K_0 = 2\sigma_{33}^{mx}\sqrt{\pi a}/\pi$ is the stress intensity factor due to remote loading σ_{33}^{mx}, without the

presence of fiber bridging. The energy release rate can be readily evaluated from the SIF (Tada *et al.*, 1985),

$$G(\phi) = \frac{1-\nu_m^2}{E_m}[K(\phi)]^2. \tag{40}$$

5.2. *Simplified solutions*

Simplification of the solution for the fiber-bridged crack system can be achieved if the bridging force variation inside each fiber is small such that

$$\sigma_i(\rho_0, \phi_0) = \sigma_i = \text{constant} \tag{41}$$

and the governing equation becomes

$$4\left[\left(\frac{a}{a_f}\right)^2 - \left(\frac{\rho}{a_f}\right)^2\right]^{1/2} - \frac{2}{\pi}\sum_{i=1}^{N}\frac{\sigma_i}{\sigma_{33}^{mx}}\iint_{S_i}\tan^{-1}\left(\frac{\eta}{R}\right)\frac{\rho_0\,\mathrm{d}\rho_0\,\mathrm{d}\phi_0}{Ra_f} = \xi\sigma_j$$

$$(\rho, \phi) \in S_j, j = 1, \ldots, N. \tag{42}$$

If the area S_i of each fiber is also very small compared to that of the penny-shaped crack, or $a/a_f \gg 1$ (a_f is the characteristic fiber radius), the equation can be approximately satisfied by collocating (ρ, ϕ) at only one particular point inside each fiber. If the choice of that collocation point is made at the centers, $(\rho_j\phi_j)$, of each fiber, along with the approximation of integrals, we obtain

$$4\left[\left(\frac{a}{a_f}\right)^2 - \left(\frac{\rho_j}{a}\right)^2\right]^{1/2} - \sum_{i=1}^{N} I_{ij}\frac{\sigma_i}{\sigma_{33}^{mx}} = \xi\sigma_j \quad j = 1, \ldots, N \tag{43}$$

where

$$I_{ij} = 2\frac{a_f}{R_{ij}}\tan^{-1}\frac{\eta_{ij}}{R_{ij}} \quad \text{for } i \neq j \tag{44}$$

and

$$R_{ij} = [\rho_j^2 + \rho_i^2 - 2\rho_i\rho_j\cos(\phi_j - \phi_i)]^{1/2} \quad \text{for } i \neq j \tag{45}$$

$$\eta_{ij} = \frac{[(a^2-\rho_j^2)(a^2-\rho_i^2)]^{1/2}}{a} \tag{46}$$

and

$$I_{ij} = \frac{2}{\pi}\iint_{S_i}\tan^{-1}\left(\frac{\eta}{R}\right)\frac{\rho_0\,\mathrm{d}\rho_0\,\mathrm{d}\phi_0}{Ra} \tag{47}$$

where a coordinate transformation similar to that given in eqn (38) is required to eliminate the singularity, ensuring the accurate evaluation of I_{ij} for $i = j$. From eqn (43) or its parent form, eqn (35), we can identify the following three major factors that affect a bridged-crack system: (1) the dimensionless configuration constant, as characterized by K/Ha in the case of a linear bridge; (2) the fiber distribution patterns as represented by ρ_i/a and ϕ_i; and (3) the ratio of crack to fiber radius.

The simplification presented here reduces the solution to a minimum size, allowing closed-form solutions for certain fiber distribution patterns. For example, we consider a penny-shaped crack bridged by six symmetric fibers. In this case, all the fibers have equal bridging transactions of σ_i/σ_0 $(=\sigma_2/\sigma_0, \ldots, \sigma_6/\sigma_0)$. Equation (43) becomes

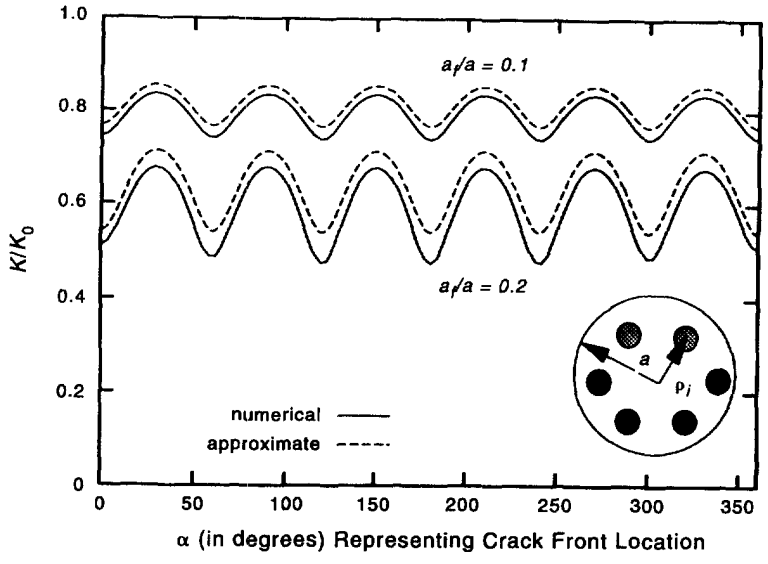

Fig. 6. The full numerical solution versus the simplified solution: six fibers (see inset) are symmetrically distributed; the distance between the centers of the fibers and the penny-shaped crack is taken as $0.7a$.

$$4\left[\left(\frac{a}{a_f}\right)^2-\left(\frac{\rho_1}{a}\right)^2\right]^{1/2}-\left(\sum_{i=1}^{6} I_{i1}\right)\frac{\sigma_1}{\sigma_0}=\xi\frac{\sigma_1}{\sigma_0}. \tag{48}$$

The bridging traction can be given in the closed form as

$$\frac{\sigma_1}{\sigma_0}=\frac{4\left[\left(\frac{a}{a_f}\right)^2-\left(\frac{\rho_1}{a_f}\right)^2\right]^{1/2}}{\xi+\sum_{i=1}^{6} I_{i1}}. \tag{49}$$

It is emphasized here that the simplified solution presented in this section is valid when the fiber radius is small compared to the penny-shaped crack's size. Figure 6 shows the variation of normalized stress intensity factors (SIFs) along the crack front for the fiber distribution pattern shown in the inset. The dotted line is the solution obtained by the simplified analysis and the solid line is the exact numerical solution. The simplified solution has an error of less than 4.5% for $a_f/a = 0.2$ (or a volume fraction of about 24%). Our numerical results for number of fiber distribution patterns show that the simplified solution can yield results with an error of less than 15% for fiber volume fractions as much as 50%. Therefore, use of the simplified solution can be justified for the most commonly used fiber-reinforced composite systems.

5.3. *Numerical results*

In this section, we examine the effect of crack size of the overall elastic moduli. With the numerical solution of bridging transitions in hand, one can easily evaluate the energy release rate through eqns (39) and (40). It is important to note that the energy release rate varies along the crack front (a function of the local polar angle, ϕ). The effective moduli are determined in a statistical averaging sense. In order to be consistent with the statistical nature of micromechanics presented in Section 3, our numerical procedure is implemented as follows: generate a distribution of fibers inside a penny-shaped crack of a given size, solve the bridging tractions via the full numerical solution outlined in Section 5.1, and evaluate the energy release rate through eqns (39) and (40). This process is repeated for a sufficient number of fiber distributions, and a statistically averaged energy release rate can

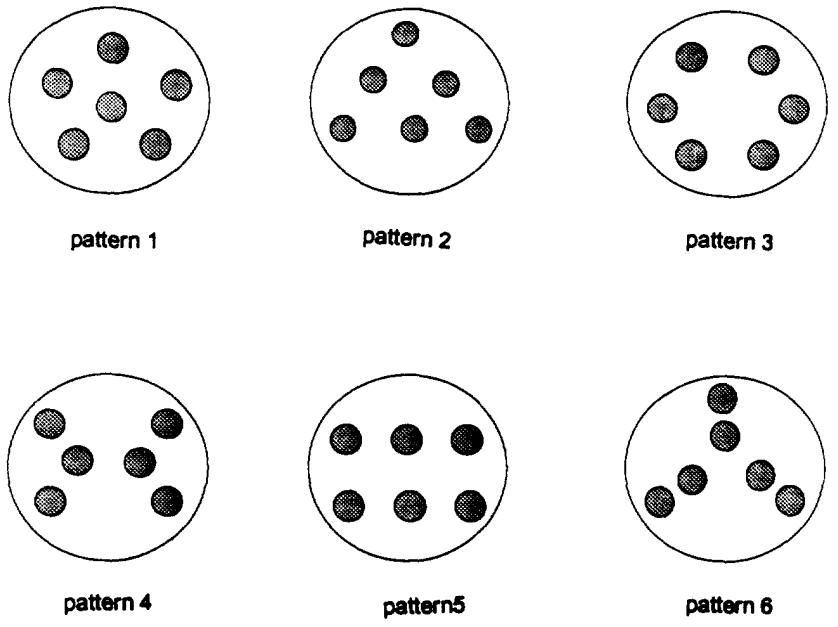

Fig. 7. Six different fiber distribution patterns.

be obtained over all the fiber distributions. After the relation of energy release rate to crack size is obtained, the effective moduli can be obtained through eqn (6).

We first consider the effect of fiber distribution on the spatial variation of fracture front behavior. The fiber distribution may vary dramatically inside a penny-shaped crack, reflecting the complexity of processing and the statistical nature of the location of crack nucleation. The widely different fiber distributions can be characterized by the distribution pattern and the average fiber spacing. The fiber distribution pattern can be particular geometrically identifiable arrangements or fully irregular arrangements. The average fiber spacing is a mathematically defined average fiber distance. In our analysis, the average fiber spacing is calculated following Huang (1993). In order to examine the effect of fiber distribution patterns on the fracture front behavior, six fiber distribution patterns with the same value for average fiber spacing, $\bar{d}/a = 0.9$, are considered in Fig. 7. As noted before, there are significant variations of SIFs along the fracture front. The average, maximum, and minimum SIFs are given in Table 1 for all six distribution patterns with $a_f/a = 2.0$ and $\xi = 0.01$. It is observed from Table 1 that, although the fiber distribution pattern can alter the maximum and minimum SIFs, it has little effect on the spatially averaged SIFs over a penny-shaped crack front. We have also conducted the calculations for several irregular fiber distribution patterns with the same $\bar{d}$ values, and the results prove that, for a given fiber spacing, the average SIFs change very little with the different patterns. This observation allows one to generate fewer statistical fiber distributions in a modeling process.

In the following, we use a SCS/Ti-6A1-4V fiber-reinforced composite as an example, with $E_m = 100$ GPa, $v_m = 0.3$, $E_f = 400$ GPa, and $v_f = 0.2$. Figure 8(a, b) considers the variation of longitudinal modulus, E_3 (in the fiber direction), with the normalized crack size, a/a_f, for a fiber volume fraction of 22.67% and 40.31%. It should be noted that crack

Table 1. SIFs of six different fiber distribution patterns with the same average spacing, $\bar{d}/a = 0.90$†

	Pattern					
	1	2	3	4	5	6
K_{avg}/K_0	0.6730	0.6702	0.6758	0.6736	0.6729	0.6878
K_{max}/K_0	0.7345	0.7615	0.7047	0.7834	0.7845	0.8089
K_{min}/K_0	0.5871	0.3949	0.6441	0.5037	0.5142	0.3763

†Dimensionless configuration constant $\xi = K/Ha_f = 0.01$.

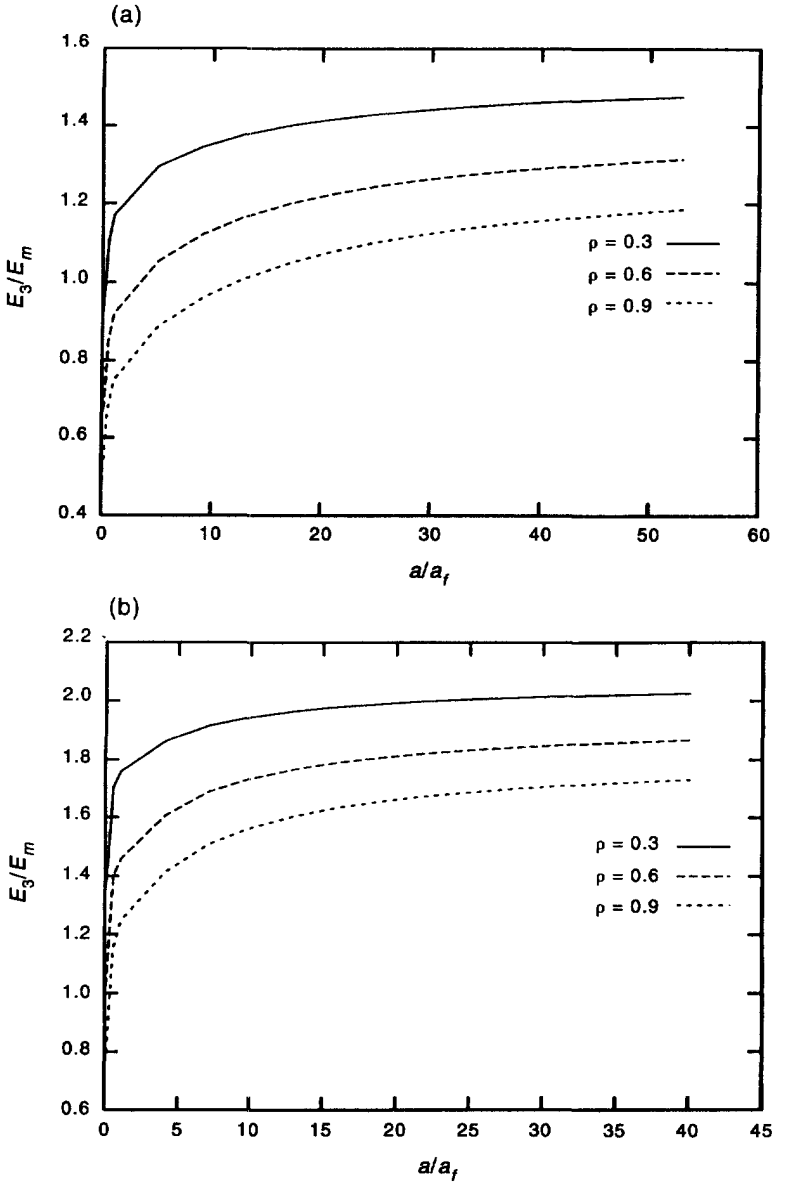

Fig. 8. Variation of longitudinal modulus, E_3/E_m, with normalized crack size, a/a_f, for a fiber-reinforced intermetallic with $E_m = 100$ GPa, $\nu_m = 0.3$, $E_f = 400$ GPa, $\nu_f = 0.2$, and $K/Ha_f = 0.01$—crack density kept fixed at $\rho = 0.3$, 0.6, or 0.9: (a) fiber volume fraction $c_f = 22.67\%$; (b) fiber volume fraction $c_f = 40.31\%$.

density is kept fixed at $\rho = 0.3$, 0.6, or 0.9. The modulus increases as crack size increases. This is due to the reasons that we conceptually described in Section 2. The bridging effect becomes significant in resisting crack opening for large-sized cracks. It is also observed that the rate of modulus increase is decreasing as crack size increases. The modulus becomes stable, or crack size insensitive, when the crack size exceeds a certain critical value. The crack-size-sensitive range depends on fiber volume fraction. For example, the modulus is sensitive to crack size when a/a_f is less than 10 for a fiber volume fraction of $c_f = 22.67\%$ and when a/a_f is less than 30 for a fiber volume fraction of $c_f = 40.31\%$. The saturated crack size can be determined approximately in these cases as $a = 10a_f$ and $a = 30a_f$. These figures also explain the necessity of the introduced scaling constant, a/a_f, for the characterization of fiber-reinforced composites. In most fiber-reinforced composites, including ceramic and intermetallic composites, the defect size mostly falls in the crack-size-sensitive range $a/a_f < 50$. For example, using photomicrographs and acoustic emission, Kim and

Pagano (1991) observed that, for several types of ceramic matrix composites with c_f between 34% and 44%, cracks of only $a = 0.2$ mm can develop before final failure, with a fiber (carbon and SiC) radius of $a_f = 8$ μm, leading to $a/a_f = 25$. This falls well within the transition range. The influence of crack size can be quite significant in that range. For instance, the standard Mori–Tanaka method gives a crack-size-independent E_3/E_m of 0.61 for a crack density of $\rho = 0.6$ and $c_f = 22.67\%$, while our crack-size-dependent prediction is 1.22 at $a/a_f = 20$ for the same crack density and fiber volume fraction. The difference is as much as 100%. Quite apparently, for the same crack density, the combination of a small number of large cracks is preferred to that of a large number of small cracks since the former offers a higher level of modulus retention.

The results presented in Fig. 8(a, b) are for the cases where fiber volume fraction and crack density (the two parameters sufficient for standard micromechanical analysis) are fixed. For a composite system sustained with matrix cracking, the crack size is physically increased, as is the crack density (as defined in eqn 2a). The information that solely reflects the modulus dependence on crack size is required in order to understand how a defect-growing process changes the composite's overall responses. This information is shown in Fig. 9(a) and (b) for fiber volume fractions of $c_f = 20.67\%$ and 40.31%, respectively. Also shown in the figures are the solutions from the standard Mori–Tanaka method (without considering bridging). In these cases, the number of cracks per unit composite volume is fixed at $N/V = 0.01$. It is observed that the modulus decreases as crack size increases. This is due to the fact that crack density increases rapidly at the power 3 of the crack size. Bridging effect is also significant in these cases. For example, the solution for bridged cracks gives $E_3/E_m = 1.75$ while the standard Mori–Tanaka method predicts $E_3/E_m = 0.85$ at $a/a_f = 20$ and $c_f = 40.31\%$.

The modulus' dependence on the dimensionless configuration constant is investigated in Fig. 10. It is observed that bridging becomes ineffective when $\xi = (K/Ha_f) > 100$. On the other hand, a further decrease in ξ does not enhance the effective modulus after the value of ξ reaches 1.0. Only within a range of ξ values between 1 and 100 is the effective modulus sensitive to the dimensionless configuration constant. For ceramic composites, the ξ value can be recovered from the fiber pull-out measurement through a simple linearization. The small ξ values require the proper level of interfacial frictions. The present analysis reveals that two other possible approaches to achieving an effective bridging are (1) to choose a matrix material with lower modulus or higher H values $[H = (1-\nu_m^2)/\pi E_m]$ and (2) to increase the fiber size. Sometimes the combination of these choices requires trade-offs to be made. From the numerical results of Fig. 10 and Table 1, we conclude that, within an effective bridging range, the effective property can be characterized solely by three parameters: fiber volume fraction, c_f; crack density, ρ; and crack size, a/a_f.

6. CONCLUSIONS AND DISCUSSION

The effective moduli of a fiber-reinforced composite with matrix cracking have been investigated in this paper. Our analysis reveals that there exist three regions that must be differentiated for the purpose of characterizing effective overall responses of a fiber-reinforced composite with matrix cracking: When the matrix crack size is infinitesimally small (or $a/a_f \to 0$), the effective moduli of the composite are a function of fiber volume fraction and crack density, and can be obtained by a standard micromechanics analysis. When the crack size is sufficiently large ($a/a_f \gg 1$ and typically > 50, or in the stable rate), the effective moduli are also only a function of fiber volume fraction and crack density and can, again, be obtained by the proposed modifications accounting for bridging effects in the context of a micromechanics analysis. When the crack size falls in a transition range ($0 < a/a_f < 50$), the effective moduli become crack size dependent and a fully bridging analysis, combined with micromechanics solution, is required for the characterization of the composite's overall responses.

The effect of fiber bridging on effective moduli was investigated in detail. Numerical results show that a standard Mori–Tanaka method can lead to underestimation of effective moduli by more than 100% as compared to our crack-size-dependent analysis. Our full

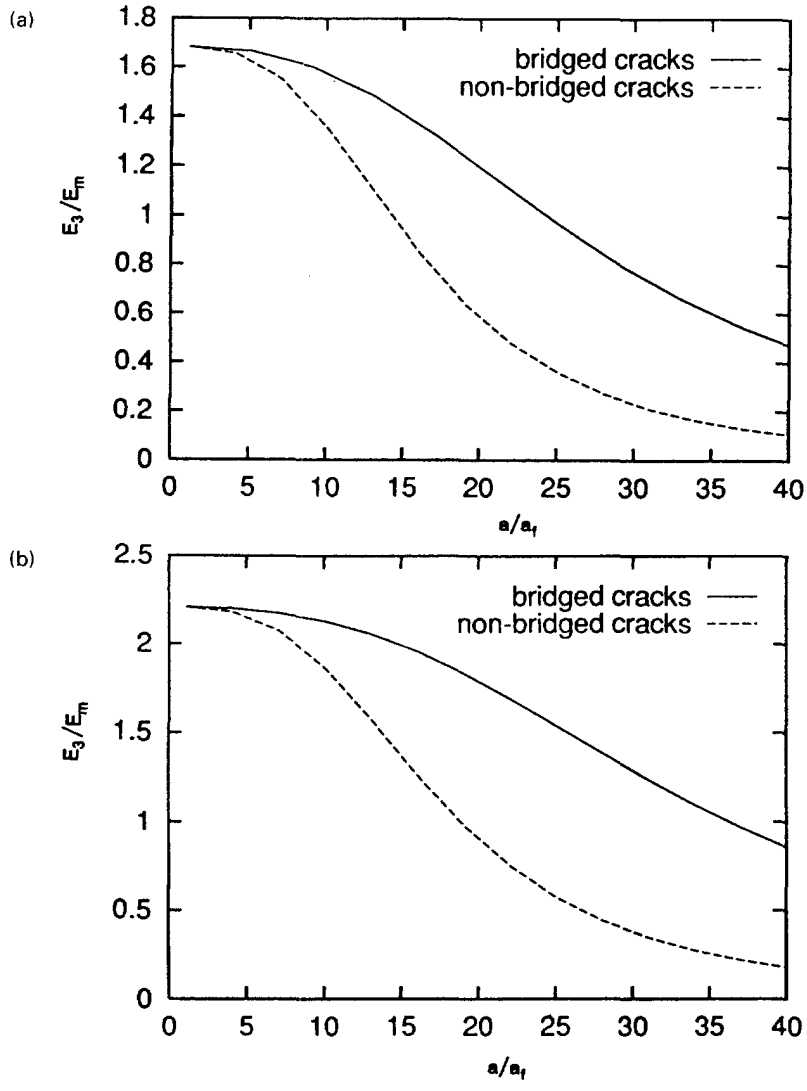

Fig. 9. Variation of longitudinal modulus, E_3/E_m, with normalized crack size, a/a_f, for a fiber-reinforced intermetallic with $E_m = 100$ GPa, $\nu_m = 0.3$, $E_f = 400$ GPa, $\nu_f = 0.2$, and $K/Ha_f = 0.01$—crack density increases according to definition in eqn (2a): (a) fiber volume fraction $c_f = 22.67\%$; (b) fiber volume fraction $c_f = 40.31\%$.

bridging analysis is based on a three-dimensional (not axisymmetrical), discrete fiber, penny-shaped crack model. In spite of the complexity involved in such a modeling process, the effective responses can still be determined entirely by three parameters within the effective bridging range: fiber volume fraction, c_f; crack density, ρ; and crack size, a/a_f. The three-parameter model also provides a convenient avenue for estimating microscale damage state from observations of overall moduli in the intermediate range ($0 < a \leqslant a_s$), which may be the regime of practical interest (Subhash and Nemat-Nasser, 1993) for many applications.

The micromechanics modification we presented for the stable range is based on bridging tractions that are self-consistent to average fiber stresses obtained by a micromechanical analysis. One possible refinement is to use the bridging traction that accounts for the axial stress variation. Our full bridging analysis also has potential applications in the analysis of toughening mechanisms (local behavior) for fiber-reinforced composites due to its distinct feature of providing spatial variations of stress intensity factors and due to its ability to account for local fiber–fiber and fiber–matrix interactions. Also, the current analysis can be easily extended to investigate the effects of particulate bridging in other types of composite materials.

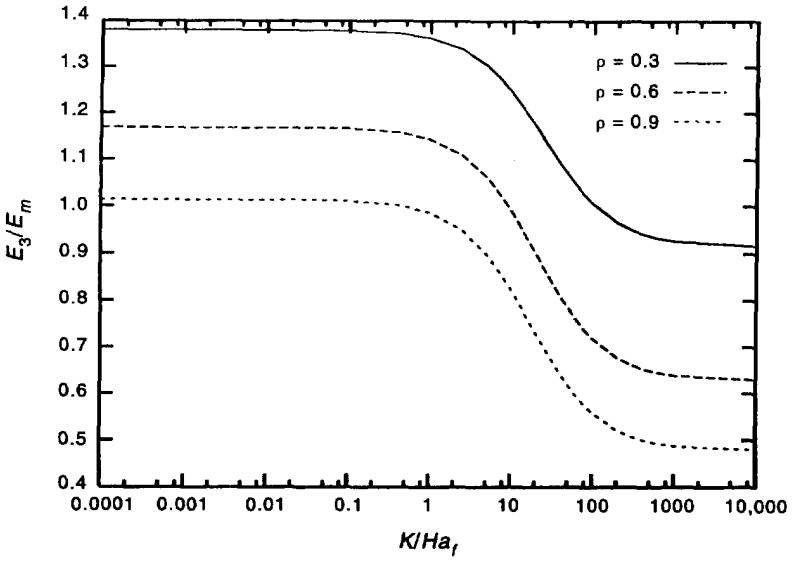

Fig. 10. The variation of longitudinal modulus, E_3/E_m, with the dimensionless constant, K/Ha_f, with $E_m = 100$ GPa, $\nu_m = 0.3$, $E_f = 400$ GPa, $\nu_f = 0.2$, fiber volume fraction $c_f = 22.67\%$, and crack size $a/a_f = 11.0$.

Acknowledgements—A. Chandra and Y. Huang gratefully acknowledge the financial support provided by Grant no. CMS9522147 from the U.S. National Science Foundation.

REFERENCES

Aveston, J., Cooper, G. A. and Kelly, A. (1971). Single and multiple fracture. In *Proceedings of the Conference on the Properties of Fiber Composites*, pp. 15–26. IPC Science and Technology Press, Guildford, U.K.

Bao, G. and Suo, Z. (1992). Remarks on crack-bridging concepts. *Applied Mechanics Review* **45,** 355–366.

Benveniste, Y. (1986). On the effective thermal conductivity of multi-phase composites. *ZAMP* **37,** 696–713.

Benveniste, Y. (1987). A new approach to the application of Mori–Tanaka's theory in composite materials. *Mechanics of Materials* **6,** 147–157.

Benveniste, Y. (1992). Uniform fields and universal relations in piezoelectric composites. *Journal of the Mechanics and Physics of Solids* **40,** 1295–1312.

Benveniste, Y. (1993). Exact results in the micromechanics of fibrous piezoelectric composites exhibiting pyroelectricity. *Proceedings of the Royal Society of London A* **441,** 59–81.

Benveniste, Y. and Dvorak, G. J. (1992). Uniform fields and universal relations in piezoelectric composites. *Journal of the Mechanics and Physics of Solids* **40,** 1295–1312.

Budiansky, B. (1965). On the elastic moduli of some heterogeneous material. *Journal of the Mechanics and Physics of Solids* **13,** 223–227.

Budiansky, B., Amazigo, J. C. and Evans, A. G. (1988). Small-scale crack bridging and the fracture toughness of particulate-reinforced ceramics. *Journal of the Mechanics and Physics of Solids* **36,** 167–187.

Budiansky, B. and O'Connell, R. J. (1976). Elastic moduli of a cracked solid. *International Journal of Solids and Structures* **12,** 81–97.

Chandra, A., Huang, Y., Wei, X. and Hu, K. X. (1995a). A hybrid micro-macro BEM formulation for micro-crack clusters in elastic components. *International Journal of Numerical Methods in Engineering* **38,** 1215–1236.

Chandra, A., Hu, K. X. and Huang, Y. (1995b). A hybrid BEM formation for multiple cracks in orthotropic elastic components, Computers and Structures **56,** 5, 785–797.

Cherepanov, G. P. (1979). *Mechanics of Brittle Fracture.* McGraw-Hill, New York.

Christensen, R. M. (1990). A critical evaluation for a class of micro-mechanics models. *Journal of Mechanics and Physics of Solids* **38,** 379–404.

Christensen, R. M. and Lo, K. H. (1979). Solutions for effective shear properties in three phase sphere and cylinder models. *Journal of Mechanics and Physics of Solids* **27,** 315–330.

Christensen, R., Schantz, H. and Shapiro, J. (1992). On the range of validity of the Mori–Tanaka method. *Journal of Mechanics and Physics of Solids* **40,** 69–73.

Deve, H. E., Evans, A. G. and Shih, D. (1992). A high-toughness gamma-titanium aluminide. *Acta Metallica* **40,** 1259–1265.

Deve, H. E. and Maloney, M. J. (1991). On the toughening of intermetallics with ductile fibers: the role of interfaces. *Acta Metallica* **39,** 2275–2284.

Dvorak, G. J. (1986). Thermal expansion of elastic–plastic composite materials. *Journal of Applied Mechanics* **53,** 737–743.

Dvorak, G. J. (1990). On uniform fields in heterogeneous media. *Proceedings of the Royal Society of London A* **431,** 89–110.

Evans, A. G. (1990). Perspective on the development of high-toughness ceramics. *Journal of the American Ceramic Society* **73,** 187–206.

Evans, A. G. and McMeeking, R. M. (1986). On the toughening of ceramics by strong reinforcements. *Acta Metallica* **34,** 2435–2441.

Fabrikant, V. I. (1989). *Application of Potential Theory in Mechanics—A Selection of New Results.* Kluwer Academic Publishers, Dordrecht, The Netherlands.

Gao, H. and Rice, J. R. (1987). Somewhat circular tensile cracks. *International Journal of Fracture* **33,** 155–174.

Hill, R. (1963). Elastic properties of reinforced solids: some theoretical principles. *Journal of the Mechanics and Physics of Solids* **11,** 357–372.

Hill, R. (1965). A self-consistent mechanics of composite materials. *Journal Mechanics and Physics of Solids* **13,** 213–222.

Hu, K. X., Chandra, A. and Huang, Y. (1994). On interacting bridged-crack systems. *International Journal of Solids and Structures* **31,** 599–611.

Huang, Y. (1993). The role of nonuniform particle distribution in plastic-flow localization. *Mechanics of Materials* **16,** 265–279.

Huang, Y., Chandra, A., Jiang, Z. Q., Wei, X. and Hu, K. X. (1996). The numerical calculation of two-dimensional effective moduli for microcracked solids. *International Journal of Solids and Structures* **33,** 1575–1586.

Huang, Y., Hu, K. X. and Chandra, A. (1993). the effective elastic moduli of microcracked composite materials. *International Journal of Solids and Structures* **30,** 1907–1918.

Huang, Y., Hu, K. X. and Chandra, A. (1994a). A generalized self-consistent mechanics method for microcracked solids. *Journal of the Mechanics and Physics of Solids* **42,** 1273–1291.

Huang, Y., Hu, K. X. and Chandra, A. (1994b). Several variations of the generalized self-consistent method for hybrid composites. *Composites Science and Technology* **52,** 19–27.

Huang, Y., Hu, K. X., Wei, X. and Chandra, A. (1994c). A generalized self-consistent mechanics method for composite materials with multiphase inclusions. *Journal of the Mechanics and Physics of Solids* **42,** 491–504.

Jiang, Z. Q., Chandra, A. and Huang, Y. (1996). A hybrid micro-macro BEM with micro-scale inclusion-crack interactions. *International Journal of Solids and Structures* **33,** 2309–2329.

Kachanov, M. (1993). Elastic solids with many cracks and related problems. In *Advanced in Applied Mechanics,* eds J. W. Hutchinson and T. Y. Wu, vol. 30, pp. 259–445. Academic Press, San Diego.

Kim, R. Y. and Pagano, N. J. (1991). Crack initiation in unidirectional brittle-material composite. *Journal of the American Ceramic Society* **74,** 1082–1090.

Marshall, D. B., Cox, B. N. and Evans, A. G. (1985). The mechanics of matrix cracking in brittle-matrix fiber composites. *Acta Metallica* **33,** 2013–2021.

McCartney, L. N. (1987). Mechanics of matrix cracking in brittle-matrix fiber-reinforced composites. *Proceedings of the Royal Society of London A* **409,** 329–350.

Mura, T. (1982). *Micromechanics of Defects in Solids,* 2nd edition. Martinus Nijhoff Publishers, The Hague, The Netherlands.

Norris, A. N. (1985). A differential scheme for the effective moduli of composites. *Mechanics of Materials* **4,** 1–16.

Roscoe, R. (1952). The viscosity of suspensions of rigid spheres. *British Journal of Applied Physics* **3,** 267–269.

Shaw, M. C., Marshall, D. B., Dadkhah, M. S. and Evans, A. G. (1993). Cracking and damage in ceramic/metal multilayers. *Acta Metallica* **41,** 3311–3322.

Siboni, G. and Benveniste, Y. (1991). A micromechanics model for the effective thermomechanical behavior of multiphase composite media. *Mechanics of Materials* **11,** 107–122.

Subhash, G. and Nemat-Nasser, S. (1993). Dynamic stress-induced transformation and texture formation in uniaxial compression of zirconia ceramics. *Journal of the American Ceramic Society* **76**(1), 153–165.

Tada, H., Paris, P. C. and Irwin, G. R. (1985). *The Stress Analysis of Cracks Handbook,* Paris Productions, Inc., St. Louis, Missouri.

Taya, M. and Chou, T.-W. (1981). On two kinds of ellipsoidal inhomogeneities in an infinite elastic body: an application to a hybrid composite. *International Journal of Solids and Structures* **17,** 553–563.

Wang, Y. M. and Weng, G. J. (1992). The influence of inclusion shape on the overall viscoelastic behavior of composites. *ASME Journal of Applied Mechanics* **59,** 510–518.

Weng, G. J. (1984). Some elastic properties of reinforced solids, with special reference to isotropic containing spherical inclusions. *International Journal of Engineering Science* **22,** 845–856.

Weng, G. J. (1990). The theoretical connection between Mori–Tanaka's theory the Hashin–Shtrikman–Walpole bounds. *International Journal of Engineering Science* **28,** 1111–1120.

Zhao, Y. H., Tandon, G. P. and Weng, G. J. (1989). Elastic moduli of a class of porous materials. *Acta Mechanica* **76,** 105–130.

Zimmerman, R. W. (1991). Elastic moduli of a solid containing spherical inclusions. *Mechanics of Materials* **12,** 17–24.